Experimental validation of a homogenized energy model for magnetic after-effects

Thomas R. Braun[a] and Ralph C. Smith[b]
Center for Research in Scientific Computation, Department of Mathematics, North Carolina State University, Raleigh, North Carolina 27695-8205

Marcelo J. Dapino[c]
Department of Mechanical Engineering, The Ohio State University, Columbus, Ohio 43210

(Received 27 June 2005; accepted 23 February 2006; published online 23 March 2006)

In this letter, we experimentally validate the ability of a recently developed ferromagnetic hysteresis model to characterize magnetic after-effects in ferromagnetic materials. The modeling framework, which combines energy analysis at the lattice level with stochastic homogenization techniques to accommodate material, stress, and field nonhomogeneities, quantifies after-effects through a balance of the Gibbs and relative thermal energies. Attributes of the framework are illustrated through fits to experimental steel data. © *2006 American Institute of Physics*. [DOI: 10.1063/1.2188595]

Magnetic after-effects due to either thermally induced switching or atomic diffusion produce drift or creep in the magnetization or induction for a number of operating regimes.[1,2] Quantification of these effects is important both for accurate material characterization and the design of sensors and actuators required to achieve and maintain highly accurate tolerances.

In a recently developed framework for quantifying hysteresis inherent to ferromagnetic materials, magnetic after-effects are incorporated by balancing the Gibbs and relative thermal energies at the lattice level using Boltzmann principles. The effects of polycrystallinity, material nonhomogeneities, and variable interaction fields are subsequently incorporated by assuming that local coercive and interaction fields are manifestations of underlying distributions rather than constant coefficients. The development of this framework is provided in Refs. 3–5. Experimental validation for operating regimes in which magnetic after-effects are negligible are also provided in therein. In this letter, we illustrate the ability of the model to quantify after-effects through fits of experimental steel data.

As detailed in Refs. 3–5, the macroscopic magnetization is quantified by the relation

$$M = \int_0^\infty \int_{-\infty}^\infty \nu_1(H_c)\nu_2(H_I)[\overline{M}(H+H_I;H_c)]dH_I dH_c, \quad (1)$$

or the approximate expression

$$M = \sum_{i=1}^{N_i}\sum_{j=1}^{N_j} \nu_1(H_{c_i})\nu_2(H_{I_j})[\overline{M}(H_{I_j}+H;H_{c_i})]v_i w_j, \quad (2)$$

in the homogenized energy framework. Here, ν_1 and ν_2 denote the densities for the local coercive field H_c and interaction field H_I. The abscissas associated with the quadrature formula under consideration are denoted by H_{I_j}, H_{c_i} and the quadrature weights are given by v_i, w_j. To construct the model, one can treat the density values $\{\nu_1(H_{c_i}), \nu_2(H_{I_j})\}$ as parameters to be identified through a least-squares fit to data or assume parameterized or functional representations. Since a negative coercive field value is nonphysical, ν_1 must be strictly positive. Further, the distribution of interactions ν_2 must be symmetric about zero, and both distributions must be bounded by a decaying exponential. Any pair of distributions which meet these three requirements are a valid choice. A reasonable example is given by

$$\nu_1(H_c) = c_1 e^{-[\ln(H_c/\overline{H}_c)/2c]^2}, \quad \nu_2(H_I) = c_2 e^{-H_I^2/2b^2}, \quad (3)$$

though other choices may yield better accuracy for some materials.

The kernel or hysteron is given by

$$\overline{M} = x_+\langle M_+\rangle + x_-\langle M_-\rangle, \quad (4)$$

where x_- and x_+, respectively, denote the fractions of moments having negative and positive orientations and

$$\langle M_-\rangle = \int_{-\infty}^{M_0} M\mu(G)dM, \quad \langle M_+\rangle = \int_{M_0}^{\infty} M\mu(G)dM, \quad (5)$$

are the associated average magnetizations. In practice, these are typically approximated by using the inflection point $\pm M_I$ instead of the unstable equilibrium M_0, as discussed in Ref. 3. These choices are further motivated by the observation that if one considers the forces $\frac{\partial G}{\partial M}$ due to the applied field, the maximal restoring forces occur at M_I and $-M_I$ as detailed on pages 332–333 of Ref. 2. This simplifies calculation and does not greatly affect accuracy. In Eq. (5), the Gibbs energy is given by

$$G(H,M) = \psi(M) - \mu_0 HM, \quad (6)$$

where

$$\psi(M) = \begin{cases} \frac{1}{2}\eta(M+M_R)^2, & M \leqslant -M_I \\ \frac{1}{2}\eta(M-M_R)^2, & M \geqslant M_I \\ \frac{1}{2}\eta(M_I-M_R)\left(\frac{M^2}{M_I}-M_R\right), & |M| < M_I \end{cases} \quad (7)$$

denotes the Helmholtz energy and μ_0 is the permeability of free space. The derivation of this energy is given in Ref. 3. Here, M_I, M_R, and η, respectively, denote the positive inflection point in the piecewise definition of ψ, the local rema-

[a]Electronic mail: trbraun@unity.ncsu.edu
[b]Electronic mail: rsmith@eos.ncsu.edu
[c]Electronic mail: dapino.1@osu.edu

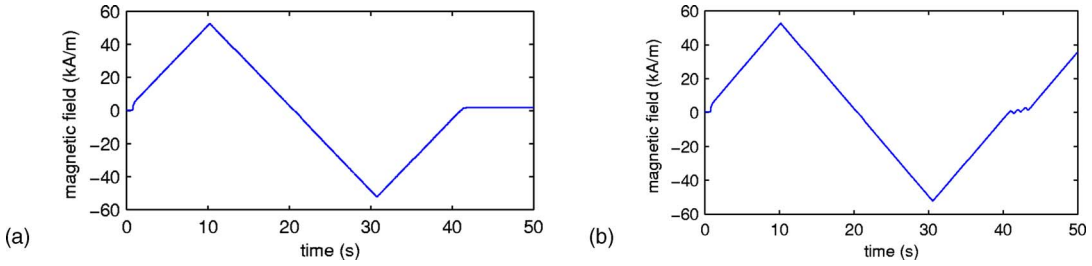

FIG. 1. (a) Input magnetic field for creep data. (b) Input magnetic field for symmetric major and biased minor loops.

nence magnetization delineating a minimum of ψ, and the inverse magnetic susceptibility after switching. The probability of attaining a given Gibbs energy level is quantified by Boltzmann's relation

$$\mu(G) = \mathcal{C}e^{-GV/kT} \tag{8}$$

which balances G with the relative thermal energy kT/V where k, T, and V, respectively, denote Boltzmann's constant, temperature in degrees Kelvin, and a reference volume. Given the identity $x_+ + x_- = 1$, the moment fractions may be computed by the differential equation

$$\dot{x}_+ = -p_{+-}x_+ + p_{-+}(1 - x_+). \tag{9}$$

Here, p_{+-} and p_{-+}, respectively, denote the likelihoods that moments switch from positive to negative, and conversely. The first likelihood is given by

$$p_{+-} = \frac{1}{\mathcal{T}} \frac{\int_{M_I-\epsilon}^{M_I+\epsilon} e^{-G(H,M)V/kT} dM}{\int_{M_I-\epsilon}^{\infty} e^{-G(H,M)V/kT} dM}, \tag{10}$$

where ϵ is a small positive constant and $\mathcal{T}$ denotes the material-dependent relaxation time so that $\omega = \frac{1}{\mathcal{T}}$ quantifies the frequency at which moments attempt to switch. The use of M_I rather than M_0 is motivated in a manner analogous to that discussed after Eq. (5) and hence the numerator specifies the field at which the stable local minimum is eliminated whereas the denominator quantifies all admissible positive magnetization values. The equation for p_{-+} is analogous. As detailed in Ref. 3, approximation of Eq. (10) with point evaluation ($e^{-G(H,M_I)V/kT}$) in the numerator is sometimes employed as well. This yields nearly identical model predictions but must be interpreted as approximate from a statistical sense.

One manifestation of magnetic after-effects is that the magnetization of the material may continue to change for a period of time after the input magnetic field is held constant. This is commonly referred to as creep and it must be dealt with in any application where the magnetization is held constant for longer than the relaxation time $\mathcal{T}$. Magnetic after-effects can also significantly change the shape of biased minor hysteresis loops, which must be handled for accurate device characterization and control design.

It is these two manifestations that we characterize through fits and predications with experimental steel data. The fields plotted in Fig. 1 were input to a cylindrical steel rod measuring 2.0 in. by 0.25 in., yielding the magnetization profiles shown in Figs. 2–4. The scalar parameters η, kT/V, and $\mathcal{T}$, as well as the densities ν_1 and ν_2 were estimated by a least squares fit to the measured data, using four point Newton-Cotes quadrature with seven quadrature intervals. For computational efficiency, the approximation scheme given in Ref. 6 was employed.

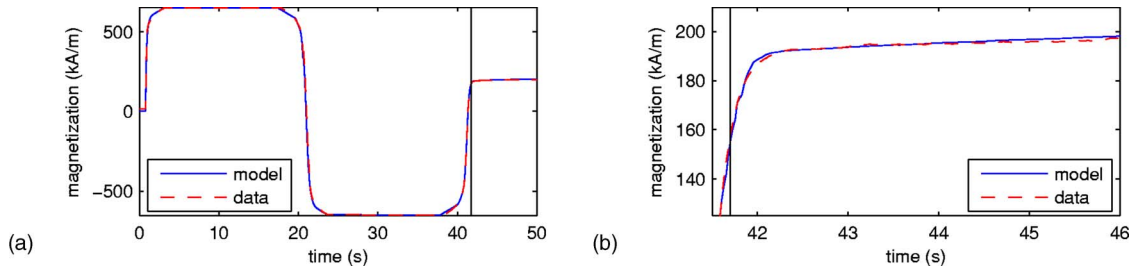

FIG. 2. (a) Model fit to the creep data where the vertical line indicates time at which the magnetic field is held constant. (b) Detailed view of creep component of the experiment and fit.

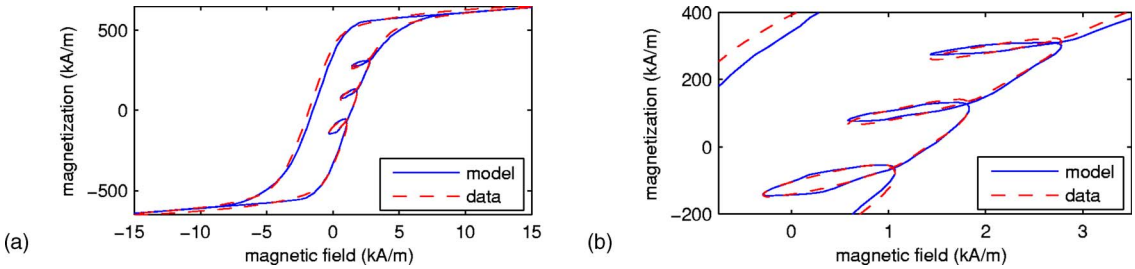

FIG. 3. Fit obtained to the (a) creep data, and (b) biased minor loop data with the model parameters estimated using the combined data set.

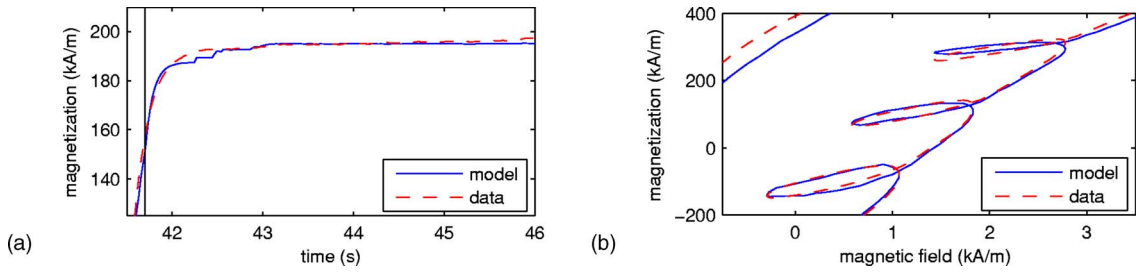

FIG. 4. (a) Model fit to symmetric major and biased minor loop data. (b) Detailed view of biased minor loop fit.

To illustrate the predictive ability of the model, we first consider separate fits to the creep and minor loop data. The model constructed through a least squares fit to the creep data [using the input in Fig. 1(a)], and giving extra weight to errors occurring immediately after the field was held constant) is compared with magnetization data in Fig. 2. The maximum error from the time the input field is held constant to the end of the interval shown in Fig. 2(b) is approximately 3 kA/m, or less than 0.5% of the saturation magnetization; the average error over the time interval is significantly less: Approximately 0.7 kA/m.

The model fit to the major and minor loop data is shown in Fig. 4, using the input field given in Fig. 1(b). When estimating parameters, errors in the biased minor loop regions were weighted more heavily than in the symmetric major loop, thus yielding more accuracy in that region of the hysteresis curve. In Fig. 3(b), it is observed that the model accurately describes the increase in magnetization following field reversal which is due to a relaxation phenomenon. The maximum error is below 13 kA/m, which is on the order of 2% of the saturation magnetization.

To illustrate the ability of the model to simultaneously characterize both phenomena, the model fit obtained with parameters estimated using the combined data set is compared with creep and biased minor loop data in Fig. 3. In this case, the creep is predicated to within 4.3 kA/m (less than 0.7% of the saturation magnetization) whereas the maximum error in the minor loops is slightly over 21 kA/m (approximately 3.25% of the saturation magnetization).

For brevity, we have focused solely on fits to steel data; however, similar accuracy has been obtained with data collected from nickel and Terfenol-D rods.

In summary, the homogenized energy framework provides the ability for quantifying magnetic after-effects as manifested in both biased minor loop operation and the magnetization response to a fixed input field following dynamic operation. The former is important for accurate material/device characterization whereas the latter is crucial for characterizing devices required to maintain a fixed magnetization or position for timescales comparable to the relaxation time of the material. In addition to device characterization, the ability of the framework to accommodate magnetic after-effects proves crucial in model-based control design for magnetic actuators operating in nonlinear and hysteretic regimes.

The research of one of the authors (R.C.S.) was supported in part through NSF Grant Nos. CMS-0099764 and CMS-0201560, and in part by the Air Force Office of Scientific Research through Grant Nos. AFOSR-F49620-01-1-0107 and AFOSR-FA9550-04-1-0203. The work of one author (T.R.B.) was supported by the United States Department of Education through a GAANN fellowship, and the research of another (M.J.D.) was supported in part by Ohio State University.

[1]S. Chikazumi, *Physics of Ferromagnetism*, 2nd ed. (Clarendon, Oxford, 1997).
[2]B. D. Cullity, *Introduction to Magnetic Materials* (Addison–Wesley, Reading, MA, 1972).
[3]R. C. Smith, *Smart Material Systems: Model Development* (SIAM, Philadelphia, PA, 2005).
[4]R. C. Smith, M. J. Dapino, T. R. Braun, and A. P. Mortensen, IEEE Trans. Magn. (accepted for publication).
[5]R. C. Smith, M. J. Dapino, and S. Seelecke, J. Appl. Phys. **93**, 458 (2003).
[6]T. R. Braun and R. C. Smith, Proc. SPIE **5757**, 377 (2005).